Dicke State Generation and Extreme Spin Squeezing via Rapid Adiabatic Passage

Sebastian C. Carrasco[®], ^{1,*} Michael H. Goerz[®], ¹ Svetlana A. Malinovskaya[®], ² Vladan Vuletic[®], ³ Wolfgang P. Schleich[®], ⁴ and Vladimir S. Malinovsky[®] ¹ DEVCOM Army Research Laboratory, Adelphi, Maryland 20783, USA ² Department of Physics, Stevens Institute of Technology, Hoboken, New Jersey 07030, USA ³ Department of Physics, MIT-Harvard Center for Ultracold Atoms, and Research Laboratory of Electronics, Massachusetts Institute of Technology, Cambridge, Massachusetts 02139, USA ⁴ Institute of Quantum Physics and Center for Integrated Quantum Science and Technology (IQST), Ulm University, Ulm, Germany

(Received 30 May 2023; accepted 15 March 2024; published 12 April 2024)

Considering the unique energy level structure of the one-axis twisting Hamiltonian in combination with standard rotations, we propose the implementation of a rapid adiabatic passage scheme on the Dicke state basis. The method permits to drive Dicke states of the many-atom system into entangled states with maximum quantum Fisher information. The designed states allow us to overcome the classical limit of phase sensitivity in quantum metrology and sensing. We show how to generate superpositions of Dicke states, which maximize metrological gain for a Ramsey interferometric measurement. The proposed scheme is remarkably robust to variations of the driving field and has favorable time scaling, especially for a small to moderate (~1000) number of atoms, where the total time does not depend on the number of atoms.

DOI: 10.1103/PhysRevLett.132.153603

Quantum sensors have the potential to go beyond their classical counterparts [1–7] and reach the fundamental quantum precision limit, the Heisenberg limit (HL) [8,9], by fully exploiting nonclassical properties of matter. In that limit, measurement precision scales proportional to the number of atoms. In contrast, the standard quantum limit (SQL) scales proportional to the square root of the number of atoms. To achieve enhanced scaling, it is imperative to find robust ways to create ultrasensitive entangled quantum states and engineering protocols to utilize them. The quantum advantage thus obtained will boost the precision of interferometric devices such as accelerometers [10], gyroscopes [11,12], and gravimeters [13]. Further applications are the search for dark matter [14], timekeeping [15], gravitational wave detection [16], geodesy [17–19]. and ultraprecise tests of the fundamental laws of physics [20,21]—all fields where ultraprecise metrology plays the crucial role.

One common method of creating collective entanglement is through an effective one-axis twisting (OAT) Hamiltonian [22], often engineered by exploiting the nonlinear interaction between the atoms and the light inside a cavity [7,23–26]. That Hamiltonian squeezes the quantum state quasiprobability distribution, creating nonclassical correlations that reduce the variance of one measurement quadrature while increasing the variance in the orthogonal direction. Thus, squeezing can enhance precision in Ramsey interferometric measurements [27]. The maximum metrological gain in the context of Ramsey interferometry is achieved with particular squeezed states known as

extreme spin-squeezed (ESS) states [28–31]. We consider the dynamics of the system in the Dicke basis, the set of eigenstates $|S, m\rangle$ of the operator \hat{S}_z . In general, ESS states are a superposition of Dicke states, but as the squeezing increases, they gravitate to a single Dicke state.

Collective rotations generate transitions between Dicke states, which in combination with applications of the OAT Hamiltonian steer the *N*-atom system towards the desired ESS states. One widely used control scheme is to use a fixed-area resonant pulse scheme, that is, a train of Rabi pulses [32,33]. Precise control of the pulse power and duration is required for this method to be effective since errors accumulate with the pulse train [34].

An alternative is to use rapid adiabatic passage (RAP) to generate the state transitions [35–39]. In this case, the transition frequency sweeps through the resonance with the excitation frequency as in the Landau-Zener model [40], and the frequency chirp leads to a robust population transfer [41,42]. Shortcuts to adiabaticity may be used to speed up the process [43,44].

Here, we propose an implementation of the RAP method to create extreme spin-squeezed states and pure Dicke states. We consider *N* noninteracting two-level atoms or spin one-half particles under the action of the Hamiltonian

$$\hat{H} = \chi \hat{S}_z^2 + \beta(t)\hat{S}_z + \Omega(t)\hat{S}_x, \tag{1}$$

where \hat{S}_j are the components of the collective spin operator, j = x, y, z. The first term is the entangling OAT interaction, and χ is the shearing parameter. The second and third terms

are rotations around the z and x axes. We are addressing the situation in the limit where dissipation is weak, and the system is well represented by the Hamiltonian of Eq. (1). In the context of the Hamiltonian implementation using the interaction between atoms and light in a cavity, this case corresponds to the limit of very strong cavity coupling. The Hamiltonian can also be realized in superconducting qubits [45] or exploiting the Ising interactions between trapped ions [46] and Rydberg atoms [47,48].

The equation of motion for the probability amplitude being in a Dicke state $|S, m\rangle$ is

$$i\dot{a}_{m} = E_{m}(t)a_{m} + \frac{\Omega(t)}{2}(\zeta_{+}a_{m+1} + \zeta_{-}a_{m-1}),$$
 (2)

where $E_m = \chi m^2 + \beta(t)m$ is the state energy, $\zeta_{\pm} = [(S \mp m)(S \pm m + 1)]^{1/2}$ are transition elements, and m = -S, -S + 1, ..., S - 1, S for N = 2S particles. We focus here on an even number N of atoms, for which there is a unique ground state $|S, 0\rangle$ [49].

According to Eq. (2), only neighboring Dicke states are coupled. Therefore, it is possible to generate successive transitions $m=n \to n \pm 1$, or to create a superposition of several Dicke states by properly choosing the time-dependent function $\beta(t)$ in Eq. (1) and controlling the duration of the field $\Omega(t)$. For example, we can start from the coherent spin state (CSS) $|S,S\rangle$ and then use various control methods [50] to prepare a desired Dicke state or other correlated quantum states.

To evaluate the usefulness of a state for high-precision measurement, we use the quantum Fisher information (QFI) [51–53]. For pure states, the QFI of a state $|\psi\rangle$ is $\mathcal{F}_j = 4(\langle \psi | \hat{S}_j^2 | \psi \rangle - \langle \psi | \hat{S}_j | \psi \rangle^2)$, with $j=x,\ y,\ z$. For the Dicke state $|S,m\rangle$, we find $\mathcal{F}_z=0$ and $\mathcal{F}_{x,y}=4\Delta S_{x,y}^2=N^2/2-2m^2+N$. Thus, Dicke states are not sensitive to perturbations proportional to S_z (due to their axial symmetry on the Bloch sphere). In contrast, $x,\ y$ components depend on m^2 and demonstrate a scaling transition from the SQL, $\mathcal{F}_{x,y}=N$ for the $|N/2,N/2\rangle$ state (a CSS), to $\mathcal{F}_{x,y}=N^2/2+N$ for the $|N/2,0\rangle$ Dicke state. According to the Cramer-Rao bound, the maximum precision of a phase estimation is bounded by the QFI as $\Delta \varphi_{x,y,z}^2 \geq 1/\mathcal{F}_{x,y,z}$ [51]. Thus $|N/2,0\rangle$ is reaching the HL scaling for x and y (up to the prefactor 1/2) for $N\gg 1$.

To prepare the $|N/2,0\rangle$ state via RAP, we apply the linear-chirping function $\beta(t)=\alpha t u(-t)$, i.e., the chirp rate α stops at t=0 due to the Heaviside step function u(-t). In this case, the linear chirping tunes the transitions between the adjacent Dicke state to the resonance, and appropriate $\Omega(t)$ efficiently transfers population from the initial CSS to a target Dicke state or Dicke state superposition.

Figure 1 presents both the diabatic and adiabatic pictures of the multiple sequential crossings between the state energies, $E_m(t)$, which become avoided crossings due to

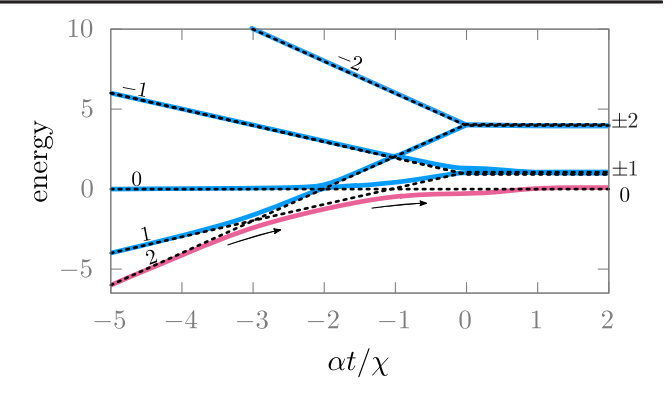


FIG. 1. Example of the energy levels of the five lowest Dicke states as a function of time. The solid lines represent the instantaneous eigenvalues of the Hamiltonian in Eq. (1) (adiabatic picture), and the dashed curves are the diagonal values, E_m , (diabatic picture). The coupling pulse goes up to $\Omega_{\rm max}=0.4\chi$. It starts to turn off at t=0 and is entirely off at $\alpha t/\chi=1$. The chirp rate is $\alpha=0.1\chi^2$.

the coupling $\Omega(t)$. The crossing time between adjacent Dicke states m and m-1 is $t_{m,m-1}=\chi(1-2m)/\alpha$, providing resonances between adjacent Dicke states with period $\tau=2\chi/\alpha$. This comes from the interplay of the quadratic and linear structure of \hat{S}_z^2 and \hat{S}_z eigenvalues, in complete analogy with the RAP between momentum states using frequency-chirped standing-wave fields [34,35].

In the adiabatic limit, each sequential avoided crossing can be considered independent, and the Dicke state population dynamics is described by the well-known Landau-Zener model [40]. Therefore, if at $t = -\infty$ the whole N-atom system population is in the CSS (single Dicke state $|N/2, N/2\rangle$), then, according to the adiabatic theorem, the total evolution of the system happens in the single adiabatic state (the lowest solid line in Fig. 1). Since the chirp stops at t=0 and the coupling $\Omega(t)$ is turned off soon after, the last avoided crossing is between the Dicke states $|N/2,1\rangle$ and $|N/2,0\rangle$. Therefore, when adiabatic conditions are satisfied for all sequential crossings, the system population will be efficiently transferred to the target Dicke state $|N/2,0\rangle$ at the final time. This qualitative picture is independent of the number of atoms, as long as adiabaticity is maintained $(\Omega_{\text{max}}^2/\alpha \gg 1)$.

In Fig. 2, we show the dynamics of the Dicke state populations using RAP from $|5,5\rangle$ to $|5,0\rangle$ with fidelity $\epsilon^2=0.9996$. To be realistic, we are turning $\Omega(t)$ on and off with a Blackman shape. The value at the plateau is $\Omega_{\rm max}=0.88\chi$. There is a residual population of the $|5,\pm 1\rangle$ states building up at the end, which returns to the target $|5,0\rangle$ state as the pulse $\Omega(t)$ is turned off. This transient effect is known as adiabatic population return for off-resonant excitation schemes [50].

The results shown in Fig. 2 are extremely robust to variations in the chirp rate α and the coupling strength $\Omega(t)$, see Supplemental Material [54]. Indeed, it is sufficient to

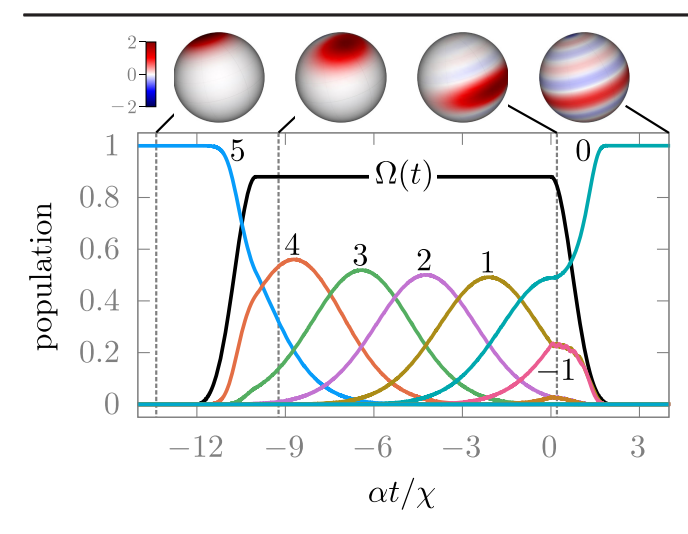


FIG. 2. Population dynamics of the ten-atom Dicke states. The solid black line shows the coupling pulse shape, $\Omega(t)$. The chirp rate is $\alpha = 0.1\chi^2$.

have a slow turn-on before the first crossing, between energies $E_5(t)$ and $E_4(t)$ of the $|5,5\rangle$ and $|5,4\rangle$ Dicke states here. We set the plateau to start at $t_1 = -N\chi/\alpha$ with a switch-on time of $t_{\rm on}=2\chi/\alpha$, and choose $t_2=0$ as the plateau end with $t_{\rm off}=2\chi/\alpha$ for the switch-off time. A time delay of the plateau end to $t_2 = \chi/\alpha$ slightly reduces the fidelity to $\epsilon^2 = 0.9992$. Increasing the number of atoms N requires only an earlier start of the plateau time by a corresponding number of periods τ to accommodate more Dicke state crossings. The adiabatic picture in Fig. 1 is valid for an arbitrary number of the atoms for the target Dicke state $|N/2, 0\rangle$. It is also possible to choose any other Dicke state as a target, which can be efficiently prepared with high fidelity by applying the same excitation scheme. To selectively prepare another Dicke state $|N/2, n\rangle$, we need to adjust the plateau duration time so that the last avoided crossing is between states $|N/2, n+1\rangle$ and $|N/2, n\rangle$.

At the top of Fig. 2, we show a Wigner representation [55,56] (see Supplemental Material [54]) of the system state on the generalized Bloch sphere at selected times. There are fringes indicating atomic coherence. Note that there is a reduced variance in the z direction at the final time. In fact, the variance $\Delta \hat{S}_z^2$ is zero for any Dicke state, including the $|N/2,0\rangle$ state. However, there is no clear orientation of the total spin, the state is symmetric in the x-y plane, and the mean spin components $\langle \hat{S}_{x,y,z} \rangle$ of the state are zero. Therefore, the standard Ramsey interferometry with this state has zero contrast. However, it is possible to design another measurement scheme that can utilize the full quantum advantage of the Dicke state $|N/2,0\rangle$ using a twist-and-turn strategy to decode the phase imprinted in the quantum state after free evolution as in [57,58].

To demonstrate the efficiency and robustness of the proposed scheme, in Fig. 3, we present the QFI

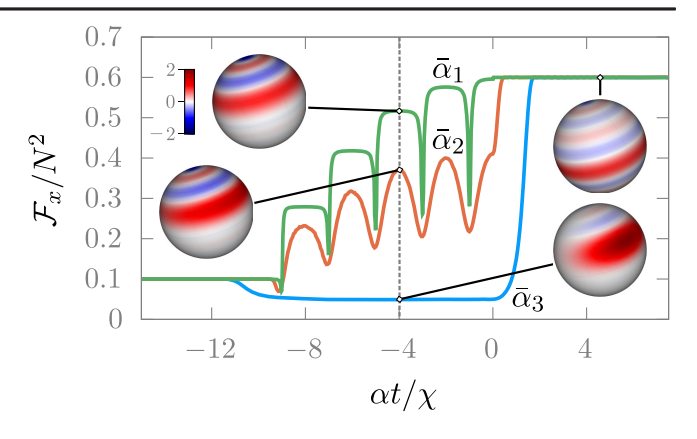


FIG. 3. Quantum Fisher information, \mathcal{F}_x , as a function of time for the RAP transfer from $|S,S\rangle$ to $|S,0\rangle$ for three values of $\bar{\alpha}=\alpha/\chi^2$, $\bar{\alpha}_1=10^{-4}$, $\bar{\alpha}_2=10^{-2}$, and $\bar{\alpha}_3=10^{-1}$; N=10. We also present snapshots of the Wigner function of the collective state at the selected time.

time-evolution during the RAP process with several values of the chirp rate. Initially, the system is in the Dicke state $|S,S\rangle$, the QFI equals N=10. The QFI dynamics depend strongly on the chirp rate, yet all regimes give the same final result. For $\alpha = 10^{-4} \chi^2$, the dynamics of the Dicke state population is fully adiabatic; the population goes sequentially from one Dicke state to the next and, at most, only two adjacent states are populated at any time. In the plateau areas, the values of the QFI correspond to the QFI of individual Dicke states, $\mathcal{F}_x = N^2/2 - 2m^2 + N$. The reduction of the QFI in this regime can be evaluated by calculating QFI for a two-Dicke-state superposition $|\psi\rangle = \cos \zeta/2|S,m\rangle +$ $e^{i\phi}\sin\zeta/2|S,m\pm1\rangle$. We find $\mathcal{F}_z=\sin^2\zeta$, $\mathcal{F}_x=N^2/2+$ $N-2m^2+2(2m\pm 1)\sin^2\zeta/2-\sin^2\zeta\cos^2\phi(N^2/4-m^2+N/2\mp m), \text{ and } \mathcal{F}_y=N^2/2+N-2m^2+2(2m\pm 1)$ $\sin^2 \zeta/2 - \sin^2 \zeta \sin^2 \phi (N^2/4 - m^2 + N/2 \mp m)$. These expressions explain the substantial reductions in the value of \mathcal{F}_x when equal superpositions are created $(\zeta = \pi/2)$, especially as m decreases. The dynamics of the QFI in the y direction, \mathcal{F}_{v} , (not shown here) is qualitatively similar and well correlated with the analytic expression above.

For larger chirp rates, $\alpha = 10^{-2}\chi^2$, more Dicke states are populated, and the QFI reduces even further at intermediate times. For $\alpha = 10^{-1}\chi^2$, we see that the QFI stays most of the time below the SQL ($\mathcal{F}_x = N$), since many Dicke states are populated simultaneously. However, a smooth switch-off of the coupling and the chirp guarantees the adiabatic passage to the target Dicke state.

A notable feature of the proposed RAP scheme is that the chirp rate α can be increased at least proportional to N (see Supplemental Material [54]). Assuming a χ independent of N, we can conclude that the total time of the RAP scheme, which is roughly $N\tau = N\chi/\alpha$, can be independent of N. Moreover, in the limit where each transition is traversed at its maximum speed, the overall time of the RAP scheme could even decrease proportionally to $\log(N)/N$. The

assumption that χ is independent of N is possible for moderate values of N (up to $N \sim 1000$) and could be accomplished by engineering the squeezing pulse, as discussed in [7,26] and the Supplemental Material [54]. In the case of larger atom numbers, χ scales as 1/N. Yet, the RAP is still efficient as long as the turn-on and off time of the coupling field is adjusted to compensate for the reduction of the energy difference between adjacent Dicke states. In that case, the total time scales as $\log(N)$ for the non-negligible values of χ .

The above-described RAP scheme can be modified to prepare another class of correlated quantum states, providing sensitivity enhancement for Ramsey spectroscopic measurements. The metrological gain can be evaluated by the Wineland squeezing parameter [59,60]

$$\xi^2 = \Delta \varphi^2 / \Delta \varphi_{\text{CSS}}^2 = \Delta \hat{S}_7^2 N / |\langle \hat{S}_x \rangle|^2, \tag{3}$$

where $\Delta \varphi^2$ is the variance of a phase estimation for an entangled state and $\Delta \varphi_{\text{CSS}}^2$ is the result for a coherent state. Here, we have chosen z as the squeezing direction and x as the mean spin orientation.

From Eq. (3), we can see that we need to minimize the quadrature in the z direction, $\Delta \hat{S}_z$, while keeping the projection onto the x axis, $\langle \hat{S}_x \rangle$, as high as possible, since it defines the maximum contrast in the interferometric protocol. It has been shown [28–31] that the optimal ESS states that minimize ξ^2 under the constraint of the fixed signal contrast must satisfy the equation $[\chi \hat{S}_z^2 - \Omega \hat{S}_x] |\Psi\rangle_{ESS} =$ $\lambda |\Psi\rangle_{ESS}$. Interestingly, as the signal contrast approaches zero, the ESS state becomes the Dicke state $|S, 0\rangle$ [29,31], and the squeezing parameter diverges. Indeed, the more metrologically useful the ESS states become, the more they approach the Dicke state $|S, 0\rangle$, and are well-approximated by a linear combination of the Dicke states $|S,0\rangle$ and $|S,\pm 1\rangle$. For a fixed value of contrast, ESS states give HL scaling [31]. Therefore, creating them allows us to achieve such scaling for Ramsey interferometry.

During the RAP generating the $|S=5,0\rangle$ Dicke state (Fig. 2), we observed transient population in the $|S=5,\pm1\rangle$ states. To create the ESS state, we abruptly turn off the coupling, $\Omega(t)$, which results in some population of the $|S,\pm1\rangle$ states at final time, thus creating the desired ESS state.

Figure 4 shows the ESS state generation via fast turn-off of the coupling during a RAP pulse aiming towards $|S,0\rangle$. The main change in the time dependence of the coupling compared to the one in Fig. 2 is that we set the switch-off time of the coupling pulse to $t_{\rm off} = 0.583\chi/\alpha$ and choose the turn-off time $t_2 = 0.5\chi/\alpha$. The maximum overlap with the ESS target state is $\epsilon^2 = 0.9994$, while the averaged spin projection onto the x axis is $\langle \hat{S}_x \rangle = S/2$. Despite these modifications, a large parameter space region still gives excellent fidelity (see Supplemental Material [54]).

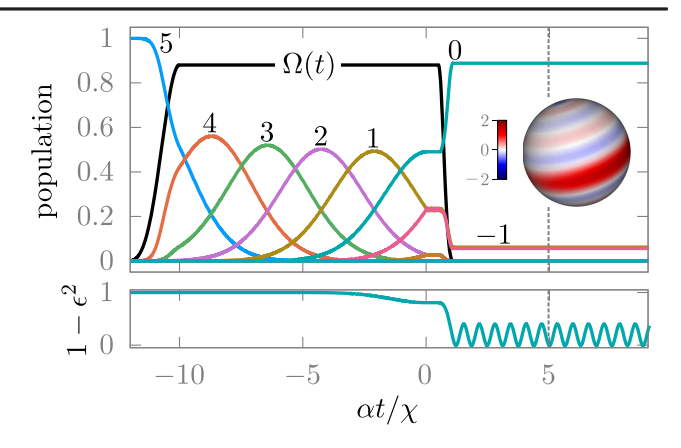


FIG. 4. Generation of the ESS state via RAP, the chirp rate is $\alpha = 0.1\chi^2$. Upper panel: the Dicke state population dynamics, the time-dependent coupling with the maximum $\Omega_{\text{max}} = 0.88\chi$ is shown by a black solid line. The Wigner function of the generated state at $t = 5\chi/\alpha$ is in the inset. Bottom panel: the infidelity as a function of time.

Since the created ESS state is not an eigenstate of \hat{S}_z^2 , which is the system's Hamiltonian after the coupling and the chirp are both turned off, the ESS state infidelity, $1 - \epsilon^2$, oscillates with the frequency proportional to the shearing strength, χ , as shown in the bottom panel of Fig. 4. The oscillations are relatively slow, and they end when turning off the OAT term in the Hamiltonian, Eq. (1), to achieve maximum fidelity. The ESS-state Wigner function is shown in the inset of Fig. 4. We observe a reduced variance in the z direction, while there is a definite orientation of the total spin $(\langle \hat{S}_x \rangle = S/2)$ that ensures significant contrast of the Ramsey signal, as opposed to the case utilizing the Dicke state $|S,0\rangle$.

So far, for illustration purposes, we have used only a small number of atoms. However, the proposed method works for arbitrary *N*. To demonstrate this, in Fig. 5, we plot the metrological gain of the RAP-produced state with

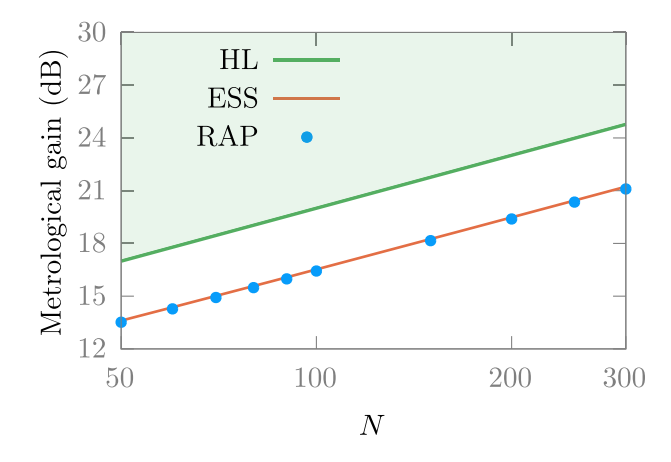


FIG. 5. Comparison between the metrological gain as a function of the atom number for ideal ESS states and ESS states created by RAP. The results share the HL scaling.

respect to the CSS. As a target state, we use an ESS state with contrast $\langle \hat{S}_x \rangle = S/2$. The metrological gain obtained with the RAP-produced states is practically identical to the ESS-state gain with the HL scaling.

To conclude, we have demonstrated the creation of manyatom entangled states via RAP between Dicke states. The generated $|S, 0\rangle$ -Dicke and ESS states maximize the QFI and metrological gain for Ramsey interferometry. We have shown how to steer the system into the Dicke state $|S,0\rangle$ and how to prepare an ESS state, providing HL scaling. The RAP technique is possible due to the unique structure of the nonlinear OAT Hamiltonian. The process is exceptionally robust to driving field variations and variations in the number of atoms, eliminating the requirement of a precise count. In addition, the total time of the RAP is independent of N for moderate N. These interesting properties open up the possibility of applying the RAP to create metrologically useful many-atom entangled states that are not easily accessible with other techniques, such as twist-and-turn strategies, that suffer from the accumulation of gates error [61] and require substantial optimization efforts [31] that become challenging to implement as N increases [32–34]. The technique could also work to prepare GHZ and various cat states. For instance, one could drive the system into $|S, -S\rangle$ (instead of $|S, 0\rangle$) and adjust the turn-on of the pulses so that the first transition only transfers half of the population, thus creating a superposition of $|S, S\rangle$ and $|S, -S\rangle$. As an extension of this work, it could be beneficial to consider a shortcut-to-adiabaticity scheme [43,44] to speed up RAP, as well as applying advanced techniques of optimal quantum control [62,63] to maximize the fidelity (and metrological gain) and minimize losses due to decoherence, dephasing, and photon scattering. The remarkable robustness of RAP may also allow for the implementation of the protocol via Ising interactions that approximate the OAT Hamiltonian [46–48], thus broadening the range of applications to other research areas.

This research was supported by DEVCOM Army Research Laboratory under Cooperative Agreements No. W911NF-24-2-0044 (S. C. C.) and No. W911NF-23-2-0128 (M. H. G.). V. S. M. is grateful for support by a Laboratory University Collaboration Initiative (LUCI) grant from OUSD. This work was supported in part by the Center of Ultracold Atoms (Grant No. PHY-2317134) and the ONR (Grant No. N00014-23-1-2577). Support is also acknowledged from the U.S. Department of Energy, Office of Science, National Quantum Information Science Research Centers, Quantum Systems Accelerator.

- [2] R. J. Sewell, M. Koschorreck, M. Napolitano, B. Dubost, N. Behbood, and M. W. Mitchell, Phys. Rev. Lett. 109, 253605 (2012).
- [3] W. Muessel, H. Strobel, D. Linnemann, D. B. Hume, and M. Oberthaler, Phys. Rev. Lett. **113**, 103004 (2014).
- [4] K. C. Cox, G. P. Greve, J. M. Weiner, and J. K. Thompson, Phys. Rev. Lett. 116, 093602 (2016).
- [5] O. Hosten, N. J. Engelsen, R. Krishnakumar, and M. A. Kasevich, Nature (London) **529**, 505 (2016).
- [6] E. Pedrozo-Peñafiel, S. Colombo, C. Shu, A. F. Adiyatullin, Z. Li, E. Mendez, B. Braverman, A. Kawasaki, D. Akamatsu, Y. Xiao, and V. Vuletić, Nature (London) 588, 414 (2020).
- [7] S. Colombo, E. Pedrozo-Peñafiel, A. F. Adiyatullin, Z. Li, E. Mendez, C. Shu, and V. Vuletić, Nat. Phys. 18, 925 (2022).
- [8] L. Pezzé and A. Smerzi, Phys. Rev. Lett. **102**, 100401 (2009).
- [9] M. Zwierz, C. A. Pérez-Delgado, and P. Kok, Phys. Rev. Lett. 105, 180402 (2010).
- [10] G. Raithel, A. Duspayev, B. Dash, S. C. Carrasco, M. H. Goerz, V. Vuletić, and V. S. Malinovsky, Quantum Sci. Technol. 8, 014001 (2022).
- [11] T. L. Gustavson, A. Landragin, and M. A. Kasevich, Classical Quantum Gravity 17, 2385 (2000).
- [12] A. Jarmola, S. Lourette, V. M. Acosta, A. G. Birdwell, P. Blümler, D. Budker, T. Ivanov, and V. S. Malinovsky, Sci. Adv. 7, eabl3840 (2021).
- [13] A. Peters, K. Y. Chung, and S. Chu, Nature (London) 400, 849 (1999).
- [14] A. Derevianko and M. Pospelov, Nat. Phys. 10, 933 (2014).
- [15] B. Guinot and E. F. Arias, Metrologia 42, S20 (2005).
- [16] S. Kolkowitz, I. Pikovski, N. Langellier, M. D. Lukin, R. L. Walsworth, and J. Ye, Phys. Rev. D 94, 124043 (2016).
- [17] T. E. Mehlstäubler, G. Grosche, C. Lisdat, P.O. Schmidt, and H. Denker, Rep. Prog. Phys. **81**, 064401 (2018).
- [18] J. Grotti, S. Koller, S. Vogt, S. Häfner, U. Sterr, C. Lisdat, H. Denker, C. Voigt, L. Timmen, A. Rolland *et al.*, Nat. Phys. **14**, 437 (2018).
- [19] M. Takamoto, I. Ushijima, N. Ohmae, T. Yahagi, K. Kokado, H. Shinkai, and H. Katori, Nat. Photonics 14, 411 (2020).
- [20] M. S. Safronova, D. Budker, D. DeMille, Derek F. Jackson Kimball, A. Derevianko, and C. W. Clark, Rev. Mod. Phys. 90, 025008 (2018).
- [21] M. S. Safronova, Ann. Phys. (Amsterdam) 531, 1970023 (2019).
- [22] M. Kitagawa and M. Ueda, Phys. Rev. A 47, 5138 (1993).
- [23] M. H. Schleier-Smith, I. D. Leroux, and V. Vuletić, Phys. Rev. A **81**, 021804(R) (2010).
- [24] I. D. Leroux, M. H. Schleier-Smith, H. Zhang, and V. Vuletić, Phys. Rev. A 85, 013803 (2012).
- [25] B. Braverman, A. Kawasaki, E. Pedrozo-Peñafiel, S. Colombo, C. Shu, Z. Li, E. Mendez, M. Yamoah, L. Salvi, D. Akamatsu, Y. Xiao, and V. Vuletić, Phys. Rev. Lett. 122, 223203 (2019).
- [26] Z. Li, B. Braverman, S. Colombo, C. Shu, A. Kawasaki, A. F. Adiyatullin, E. Pedrozo-Peñafiel, E. Mendez, and V. Vuletić, PRX Quantum 3, 020308 (2022).
- [27] J. Ma, X. Wang, C. Sun, and F. Nori, Phys. Rep. 509, 89 (2011).

^{*}seba.carrasco.m@gmail.com

T. Takano, M. Fuyama, R. Namiki, and Y. Takahashi, Phys. Rev. Lett. 102, 033601 (2009).

- [28] A. M. Bloch and A. G. Rojo, Eur. J. Control 10, 469 (2004).
- [29] G. Tóth and I. Apellaniz, J. Phys. A 47, 424006 (2014).
- [30] A. S. Sørensen and K. Mølmer, Phys. Rev. Lett. 86, 4431 (2001).
- [31] S. C. Carrasco, M. H. Goerz, Z. Li, S. Colombo, V. Vuletić, and V. S. Malinovsky, Phys. Rev. Appl. 17, 064050 (2022).
- [32] S.-W. Chiow, T. Kovachy, H.-C. Chien, and M. A. Kasevich, Phys. Rev. Lett. 107, 130403 (2011).
- [33] T. Kovachy, P. Asenbaum, C. Overstreet, C. A. Donnelly, S. M. Dickerson, A. Sugarbaker, J. M. Hogan, and M. A. Kasevich, Nature (London) 528, 530 (2015).
- [34] M. H. Goerz, M. A. Kasevich, and V. S. Malinovsky, Atoms 11, 36 (2023).
- [35] V. S. Malinovsky and P. R. Berman, Phys. Rev. A 68, 023610 (2003).
- [36] R. G. Unanyan, N. V. Vitanov, and K. Bergmann, Phys. Rev. Lett. 87, 137902 (2001).
- [37] E. Peik, M. Ben Dahan, I. Bouchoule, Y. Castin, and C. Salomon, Phys. Rev. A 55, 2989 (1997).
- [38] E. Kuznetsova, G. Liu, and S. A. Malinovskaya, Phys. Scr. T 160, 014024 (2014).
- [39] S. A. Malinovskaya, Opt. Lett. 42, 314 (2017).
- [40] J. R. Rubbmark, M. M. Kash, M. G. Littman, and D. Kleppner, Phys. Rev. A 23, 3107 (1981).
- [41] N. V. Vitanov, Phys. Rev. A 59, 988 (1999).
- [42] E. Pachniak and S. A. Malinovskaya, Sci. Rep. 11, 12980 (2021).
- [43] X. Chen, I. Lizuain, A. Ruschhaupt, D. Guéry-Odelin, and J. G. Muga, Phys. Rev. Lett. 105, 123003 (2010).
- [44] D. Guéry-Odelin, A. Ruschhaupt, A. Kiely, E. Torrontegui, S. Martínez-Garaot, and J. Muga, Rev. Mod. Phys. 91, 045001 (2019).
- [45] L. Pezzè, A. Smerzi, M. K. Oberthaler, R. Schmied, and P. Treutlein, Rev. Mod. Phys. 90, 035005 (2018).
- [46] J. Franke, S. R. Muleady, R. Kaubruegger, F. Kranzl, R. Blatt, A. M. Rey, M. K. Joshi, and C. F. Roos, Nature (London) 621, 740 (2023).
- [47] W. J. Eckner, N. Darkwah Oppong, A. Cao, A. W. Young, W. R. Milner, J. M. Robinson, J. Ye, and A. M. Kaufman, Nature (London) 621, 734 (2023).

- [48] G. Bornet, G. Emperauger, C. Chen, B. Ye, M. Block, M. Bintz, J. A. Boyd, D. Barredo, T. Comparin, F. Mezzacapo et al., Nature (London) 621, 728 (2023).
- [49] For odd N, the two lowest Dicke states $|S, \pm 1/2\rangle$ are degenerate, which affects the ESS states. Although the fundamental technique for even and odd N is the same, there are subtle differences that will be analyzed in future work.
- [50] I. R. Sola, B. Y. Chang, S. A. Malinovskaya, and V. S. Malinovsky, in *Advances in Atomic, Molecular, and Optical Physics*, edited by E. Arimondo, L. F. DiMauro, and S. F. Yelin (Academic Press, New York, 2018), Vol. 67, pp. 151–256, 10.1016/bs.aamop.2018.02.003.
- [51] S. L. Braunstein and C. M. Caves, Phys. Rev. Lett. 72, 3439 (1994).
- [52] B. M. Escher, R. L. de Matos Filho, and L. Davidovich, Nat. Phys. 7, 406 (2011).
- [53] G. Toth and I. Apellaniz, J. Phys. A 47, 424006 (2014).
- [54] See Supplemental Material at http://link.aps.org/supplemental/ 10.1103/PhysRevLett.132.153603 for a robustness analysis, numerical and analytical analysis regarding the scaling, and more information regarding the Wigner distribution.
- [55] J. P. Dowling, G. S. Agarwal, and W. P. Schleich, Phys. Rev. A 49, 4101 (1994).
- [56] B. Koczor, R. Zeier, and S. J. Glaser, Phys. Rev. A 102, 062421 (2020).
- [57] R. Kaubruegger, D. V. Vasilyev, M. Schulte, K. Hammerer, and P. Zoller, Phys. Rev. X 11, 041045 (2021).
- [58] R. Kaubruegger, A. Shankar, D. V. Vasilyev, and P. Zoller, PRX Quantum 4, 020333 (2023).
- [59] D. J. Wineland, J. J. Bollinger, W. M. Itano, F. L. Moore, and D. J. Heinzen, Phys. Rev. A 46, R6797 (1992).
- [60] D. J. Wineland, J. J. Bollinger, W. M. Itano, and D. J. Heinzen, Phys. Rev. A 50, 67 (1994).
- [61] C. D. Marciniak, T. Feldker, I. Pogorelov, R. Kaubruegger, D. V. Vasilyev, R. van Bijnen, P. Schindler, P. Zoller, R. Blatt, and T. Monz, Nature (London) 603, 604 (2022).
- [62] M. H. Goerz, S. C. Carrasco, and V. S. Malinovsky, Quantum 6, 871 (2022).
- [63] I. R. Sola, B. Y. Chang, S. A. Malinovskaya, S. C. Carrasco, and V. S. Malinovsky, J. Phys. B 55, 234002 (2022).